Environmental Science & Technology

pubs.acs.org/est

Article

Climate-Driven Harmful Algal Blooms Impair the Coastal Nitrogen Filter and Shift Denitrification Pathways toward N_2O Accumulation

Published as part of Environmental Science & Technology special issue "Safe and Just Earth System Boundaries for Novel Entities".

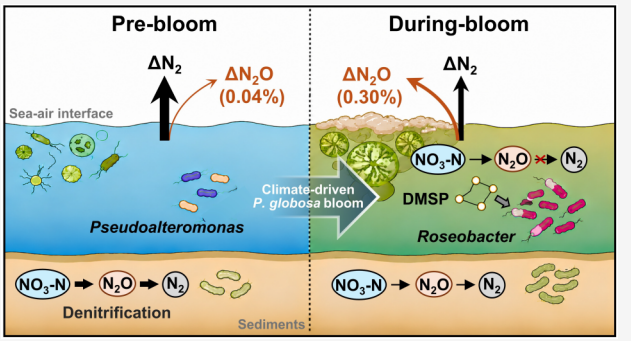
Mingzhen Zhang, Yiqi Yu, Xiyu Zhang, Fan Qu,* and Nengwang Chen*

Cite This: *Environ. Sci. Technol.* 2026, 60, 20963−20975

Read Online

ACCESS | Metrics & More | Article Recommendations | Supporting Information

ABSTRACT: Climate change is expanding harmful algal blooms (HABs) beyond nutrient-driven paradigms, yet their effects on coastal nitrogen cycling remain poorly understood. Here, we investigated a climate-driven dry-season *Phaeocystis globosa* bloom in Xiamen Bay, a subtropical coastal embayment, using field observations, isotopic incubations, and metagenomics. Contrary to the conventional view that HABs stimulate denitrification, the bloom suppressed sedimentary denitrification by ∼70% and reduced total dissolved excess gaseous nitrogen ($\Delta N_2 + \Delta N_{2r}O$) by ∼50% relative to the pre-bloom period. Despite this decline in nitrogen removal, N_2O yield ($\Delta N_2O/(\Delta N_2 + \Delta N_2O)$) increased by approximately an order of magnitude from 0.04% to 0.30%, indicating a shift toward incomplete denitrification. This shift was linked to a sulfur-mediated microbial reorganization. In seawater, sulfur-metabolizing denitrifiers, particularly *Roseobacter*, capable of utilizing algal-derived sulfur compounds (e.g., DMSP), were enriched and became dominant. These taxa harbored clade I *nosZ*, whose sensitivity to oxygen and pH likely constrained N_2O reduction. In sediments, chemolithoautotrophic sulfur-oxidizing denitrifiers, particularly *Sulfurovum*, became dominant and were associated with reduced N_2 production. Together, these compartment-specific responses weakened denitrification and shifted its end-product composition toward a higher N_2O share, revealing a sulfur-coupled microbial mechanism by which climate-driven HABs impair the coastal nitrogen filter.



KEYWORDS: *phaeocystis globosa, harmful algal blooms, nitrous oxide, denitrification, sulfur cycle*

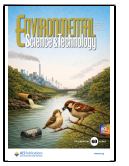
1. INTRODUCTION

Coastal phytoplankton blooms are increasing globally in frequency and scale, driven by synergistic pressures of eutrophication and climate change.[1] Among these, blooms of *Phaeocystis globosa* (*P. globosa*), a colony-forming haptophyte, pose multifaceted threats. Beyond direct impacts via hypoxia and toxin release, *P. globosa* is known to produce dimethylated sulfur compounds (e.g., DMSP, DMS) with important implications for atmospheric chemistry and climate regulation.[2,3] While the ecological and sulfur-cycle footprints of *P. globosa* are well-documented,[3−7] their cascading effects on other critical nutrient cycles, particularly the nitrogen cycle, remain a significant knowledge gap.

This knowledge gap is critical because coastal ecosystems function as a nitrogen filter, removing reactive nitrogen and mitigating eutrophication. Denitrification is the primary pathway for permanent nitrogen removal but also a major source of the potent greenhouse gas N_2O, highlighting a trade-off between nitrogen removal and climate forcing.[8,9] In this context, the prevailing paradigm is largely derived from studies of diatom- or cyanobacteria-dominant blooms in nutrient-rich systems. It posits that algal blooms generally stimulate denitrification by supplying labile organic carbon to heterotrophic denitrifiers.[10−12] Yet, this view overlooks the potential for blooms, particularly those involving atypical functional groups under emerging climatic forcing, to impair nitrogen removal efficiency and promote N_2O emissions via mechanisms such as substrate competition or microbial community restructuring.[13,14] Whether these effects manifest uniformly across the water-sediment interface remains a key uncertainty in predicting coastal feedbacks to environmental change.

Xiamen Bay, a subtropical embayment in Southeast China, presents a natural experimental setting to challenge the existing

Received: January 27, 2026
Revised: July 9, 2026
Accepted: July 9, 2026
Published: July 17, 2026



ACS Publications

© 2026 American Chemical Society

Downloaded from pubs.acs.org/esthag/article-pdf/60/30/20963/6601638/acs.est.6c01472.pdf by XIAMEN UNIV user on 16 August 2026

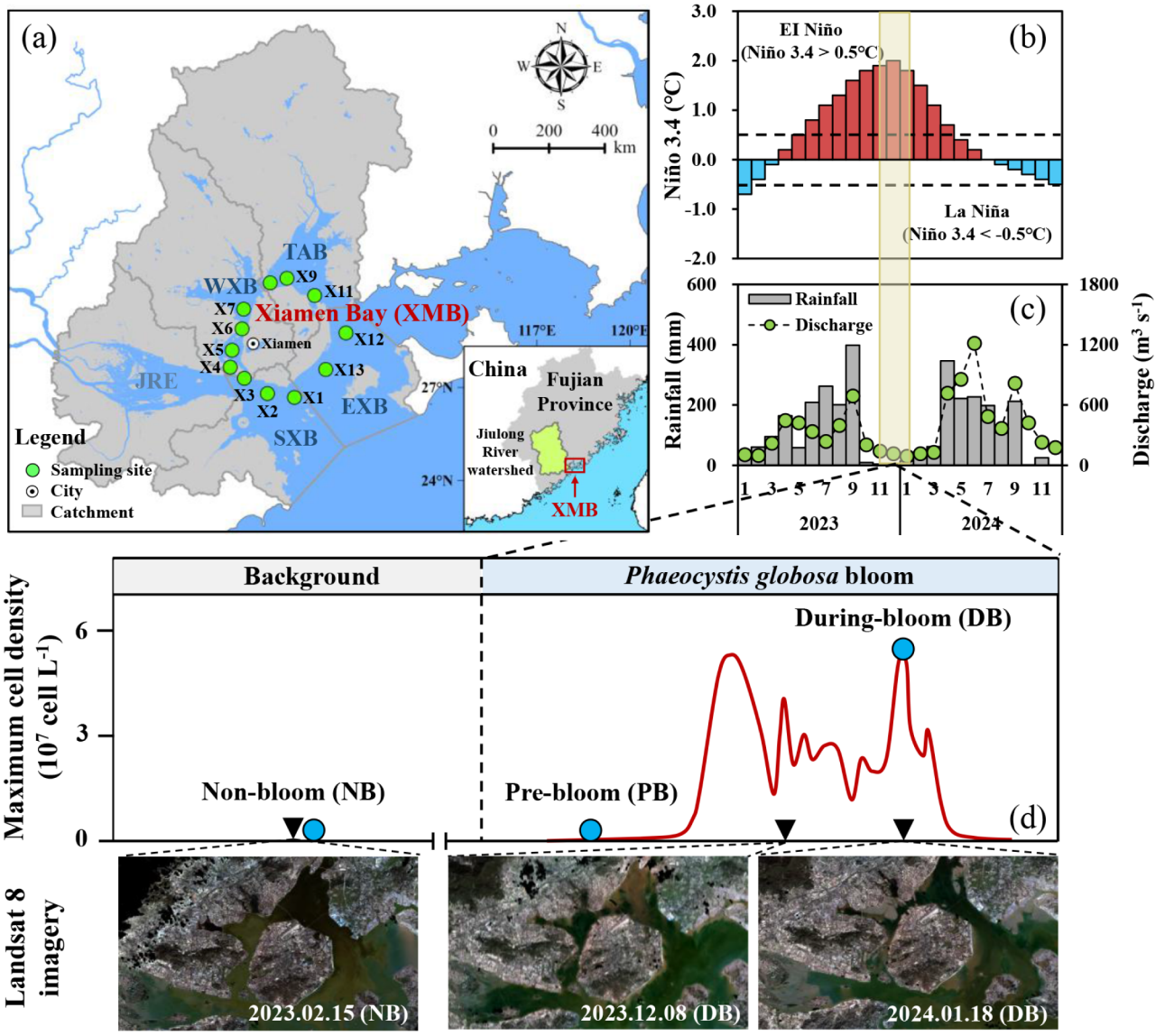


Figure 1. Study area and sampling stations during the *P. globosa* bloom in Xiamen Bay. (a) Sampling stations. (b, c) Temporal variations of Niño 3.4 index, rainfall, and river discharge. (d) Bloom timeline based on maximum cell density (red curve) with observation phases (blue circles) and satellite remote sensing images (black triangles). NB, PB, and DB refer to the non-bloom, pre-bloom, and during-bloom periods, respectively. XMB, Xiamen Bay; SXB, Southern Xiamen Bay; WXB, Western Xiamen Bay; TAB, Tong'an Bay; EXB, Eastern Xiamen Bay; JRE, Jiulong River Estuary.

paradigm. Historically, red tides in this region were confined to warm, rainy months (April−September).[15] In stark contrast, a major *P. globosa* bloom emerged unexpectedly in late November 2023 and persisted for nearly two months, marking the longest such event on record. This anomalous dry-season occurrence decouples the bloom from typical summer eutrophication patterns, implicating climate anomalies (e.g., anomalous warming) as the primary driver. This scenario provides a valuable opportunity to investigate bloom impacts on nitrogen cycling under anomalous environmental forcing.

To address the critical gaps outlined above, we conducted a field campaign spanning non-bloom (NB), pre-bloom (PB), and during-bloom (DB) periods in Xiamen Bay. We integrated in situ measurements, isotopic tracing experiments, and metagenomic analyses to test the hypothesis that a climate-driven *P. globosa* bloom occurring in the dry season would suppress complete denitrification and alter N_2O fluxes via sulfur-mediated microbial reorganization. Specifically, we aimed to (1) characterize the environmental drivers and developmental phases of this climate-driven bloom; (2) quantify its impacts on sedimentary denitrification rates and water column N_2O dynamics; and (3) mechanistically elucidate the pathways linking bloom-derived organic matter to changes in denitrifier communities and shifts in nitrogen cycling processes governing nitrogen removal and N_2O production.

2. MATERIALS AND METHODS

2.1. Study Area

Xiamen Bay is a semi-enclosed subtropical embayment located on the western coast of the Taiwan Strait, with a total marine area of ~390 km^2. The bay receives substantial freshwater input from the Jiulong River, discharging ~1.24×10^{10} m^3 of water annually into the southeastern part of the bay.[15] The river drains an agricultural catchment with historically high chemical fertilizer inputs, thereby constituting a significant source of terrestrial nutrients.[16] For analytical purposes, the bay is generally divided into four main subregions: Southern Xiamen

https://doi.org/10.1021/acs.est.6c01472
Environ. Sci. Technol. 2026, 60, 20963−20975

Downloaded from pubs.acs.org/esthag/article-pdf/60/30/20963/6601638/acs.est.6c01472.pdf by XIAMEN UNIV user on 16 August 2026

Bay (SXB), Western Xiamen Bay (WXB), Tong'an Bay (TAB), and Eastern Xiamen Bay (EXB) (Figure 1a).

The bay is relatively shallow, with an average depth of ∼10 m, and exhibits weak and transient water column stratification. The mean water residence time is 16.5 days. Hydrodynamic circulation is governed by regular semidiurnal tides and influenced by larger-scale currents, including the South China Sea Warm Current, the Kuroshio Current, and the Min-Zhe Coastal Current.[17] The regional climate has a long-term mean annual temperature of 21.6 °C and annual precipitation of 1239.1 mm, with over 85% of rainfall concentrated in the wet season from April to September.

2.2. Sampling Design and Campaign

Sampling was conducted at 12 stations distributed across the four subregions of Xiamen Bay (Figure 1a). The campaign was designed to capture the progression of a major *P. globosa* bloom, as documented in red tide bulletins issued by the Fujian Provincial Ocean and Fisheries Bureau (Figure 1d). Three sampling cruises were conducted to represent key bloom phases: Non-bloom period (NB, February 15, 2023), Pre-bloom period (PB, November 9, 2023), During-bloom period (DB, January 18, 2024). To minimize short-term tidal and operational variability, station sequence and tidal stage were held constant across cruises. Seasonal baseline variability was assessed using multiyear monitoring data (Table S1) compiled from a previously published 2019−2022 data set,[18] and extended with additional observations from 2023.

2.3. Sample Collection, Pretreatment, and Analysis

2.3.1. Field Measurements and Sample Collection. Vertical profiles of salinity, water temperature, dissolved oxygen (DO), pH, and redox potential (Eh) were measured in situ using a WTW Multi 3630 multiparameter probe. Chlorophyll *a* (Chl *a*) concentrations were determined fluorometrically on board using a Turner Designs TD-700/AquaFluor fluorometer (see Text S1 for details). Seawater samples were collected at designated depths using 5 L Niskin bottles.

2.3.2. Water Sample Processing and Storage. All seawater samples were processed immediately upon collection. For dissolved nutrients, seawater was filtered through 0.7 μm GF/F filters. One filtrate aliquot was stored at 4 °C in pre-acid-cleaned centrifuge tubes and analyzed within 1 week, while a separate aliquot was stored at −20 °C for subsequent nitrate isotope analysis. For dissolved organic matter (DOM), samples for dissolved organic carbon (DOC) were filtered through pre-combusted GF/F filters and stored at −20 °C in 40 mL amber glass vials. For chromophoric DOM (CDOM) absorption, samples were filtered through 0.2 μm polycarbonate filters (Millipore) and measured immediately. For dissolved gases, water samples for N_2O analysis were gently transferred via silicone tubing into 60 mL amber glass bottles, while 12 mL Exetainer vials were used for N_2 analysis. All containers were overflowed with at least three volumes, sealed without headspace, and stored on ice. Headspace extraction and analysis were completed within 12 h. For metagenomic analysis, a 2.5 L seawater aliquot was sequentially filtered onto 0.22 μm Isopore membrane filters (Millipore). Filters were flash-frozen and stored at −80 °C prior to processing within one month.

2.3.3. Sediment Sampling. Undisturbed sediment cores were collected using a stainless-steel box corer. The upper 0−10 cm was sectioned for microbial, physicochemical, and process-rate analyses. Samples for microbial analysis were transferred into sterile cryovials, immediately frozen, and stored at −80 °C prior to DNA extraction within one month. Samples for physicochemical analyses were processed in parallel and stored at −20 °C before analysis. Samples for nitrate reduction rate measurements were stored at 4 °C and processed within the same day of collection.

2.3.4. Laboratory Analyses. Concentrations of dissolved inorganic nutrients (NH_4−N, NO_3−N, NO_2−N, DIP, and DSi) were determined colorimetrically using a Seal AutoAnalyzer. Method detection limits were 1 μM for nitrogen species and 0.1 μM for phosphorus, with analytical precision (relative error) < 5% based on replicate analysis of 10% of samples. DOC was quantified by high-temperature catalytic oxidation using a multi N/C 3100 TOC-TN analyzer (Analytik Jena). CDOM absorption spectra (240−800 nm) were measured using a UV-2300 spectrophotometer (Techcomp), with a precision of ± 0.001 absorbance units. The $\delta^{15}N$ and $\delta^{18}O$ of nitrate were determined using the bacterial denitrifier method coupled to isotope ratio mass spectrometry (IRMS).[19] Natural abundance isotopic compositions of N_2O ($\delta^{15}N_{bulk}$, $\delta^{15}N_{\alpha}$, $\delta^{18}O$) were measured using an Isoprime-100 IRMS (Elementar) coupled to a trace-gas preconcentration unit. Dissolved N_2O concentrations were determined by gas chromatography (Agilent 7890A) following headspace equilibration. Dissolved N_2 concentrations were measured using membrane inlet mass spectrometry (MIMS, Bay Instruments).

Sediment physicochemical properties were determined using standard extraction and elemental analysis methods, as detailed in Text S2. Potential sediment nitrate reduction rates including denitrification, anaerobic ammonium oxidation (anammox), and dissimilatory nitrate reduction to ammonium (DNRA), were quantified using ^{15}N-labeled slurry incubations. Detailed protocols are provided in Texts S3 and S4. For metagenomic analysis, DNA extraction, library preparation, and paired-end sequencing (2 × 150 bp, MGI T7 platform) were conducted for 12 samples, with an average sequencing depth of ∼50 Gb per sample. Clean reads were quality-filtered and assembled using MEGAHIT. The resulting contigs were used for both gene-centric (Prodigal, DIAMOND against KEGG) and genome-centric analyses (MetaBAT2 binning). Metagenome-assembled genome (MAG) quality was assessed using CheckM2, followed by taxonomic classification with GTDB-Tk and functional annotation using KofamScan. MAG abundance was estimated based on the mean coverage of mapped reads, given the comparable sequencing depth and consistent processing across samples. Detailed procedures are provided in Texts S5−S8.

2.4. Semiquantitative Isotopic Framework for N_2O Source Partitioning and Reduction

The sources of N_2O were constrained using a dual-isotope approach combining site preference (SP) and the nitrogen isotopic difference between nitrate and N_2O ($\Delta\delta^{15}N$).[20] SP describes the intramolecular distribution of ^{15}N within the N_2O molecule, whereas $\Delta\delta^{15}N$ reflects the net isotopic offset between substrate NO_3^- and N_2O. The combined distribution in SP-$\Delta\delta^{15}N$ space enables semiquantitative discrimination between nitrification and denitrification contributions, as well as assessment of subsequent N_2O reduction. A back-calculation approach was applied to estimate the minimum contribution of nitrification and the extent of N_2O reduction, as detailed in Text S9.

2.5. Statistical and Data Analysis

Data processing, statistical analyses, and graphical visualization were performed using Microsoft Excel 2021, Origin 2024, R (version 4.2.2; RStudio Desktop), and Python (version 3.13). Details of the statistical methods and packages used are provided in Text S10.

3. RESULTS

3.1. Physicochemical Variability in Seawater and Sediments

Key physicochemical parameters of the overlying seawater exhibited pronounced temporal variations across the NB, PB, and DB periods, with minimal spatial heterogeneity. Salinity remained stable throughout the study, ranging from 29.6 ± 1.1 to 30.3 ± 1.0 (Figure S1). In contrast, water temperature, DO, pH, Eh, and Chl *a* displayed distinct phase-dependent patterns. The NB period was characterized by the lowest water temperature (15.1 ± 0.5 °C) and Chl *a* concentration (1.66 ± 0.62 μg L^{-1}). The subsequent PB period featured warmer conditions (25.0 ± 0.3 °C), a marked decrease in DO (6.91 ± 0.25 mg L^{-1}), and a significant rise in Chl *a* concentration (7.75 ± 2.84 μg L^{-1}, $p < 0.001$), indicating bloom initiation. Peak bloom conditions during DB were characterized by the highest DO (10.78 ± 0.99 mg L^{-1}), elevated pH (9.40 ± 0.32), more reduced Eh (−138.7 ± 18.0 mV), and the highest Chl *a* concentration (8.27 ± 6.36 μg L^{-1}). The spatial distributions of elevated Chl *a* during PB and DB were primarily confined to

Downloaded from pubs.acs.org/esthag/article-pdf/60/30/20963/6601463/acs.est.6c01472.pdf by XIAMEN UNIV user on 16 August 2026

https://doi.org/10.1021/acs.est.6c01472
Environ. Sci. Technol. 2026, 60, 20963−20975

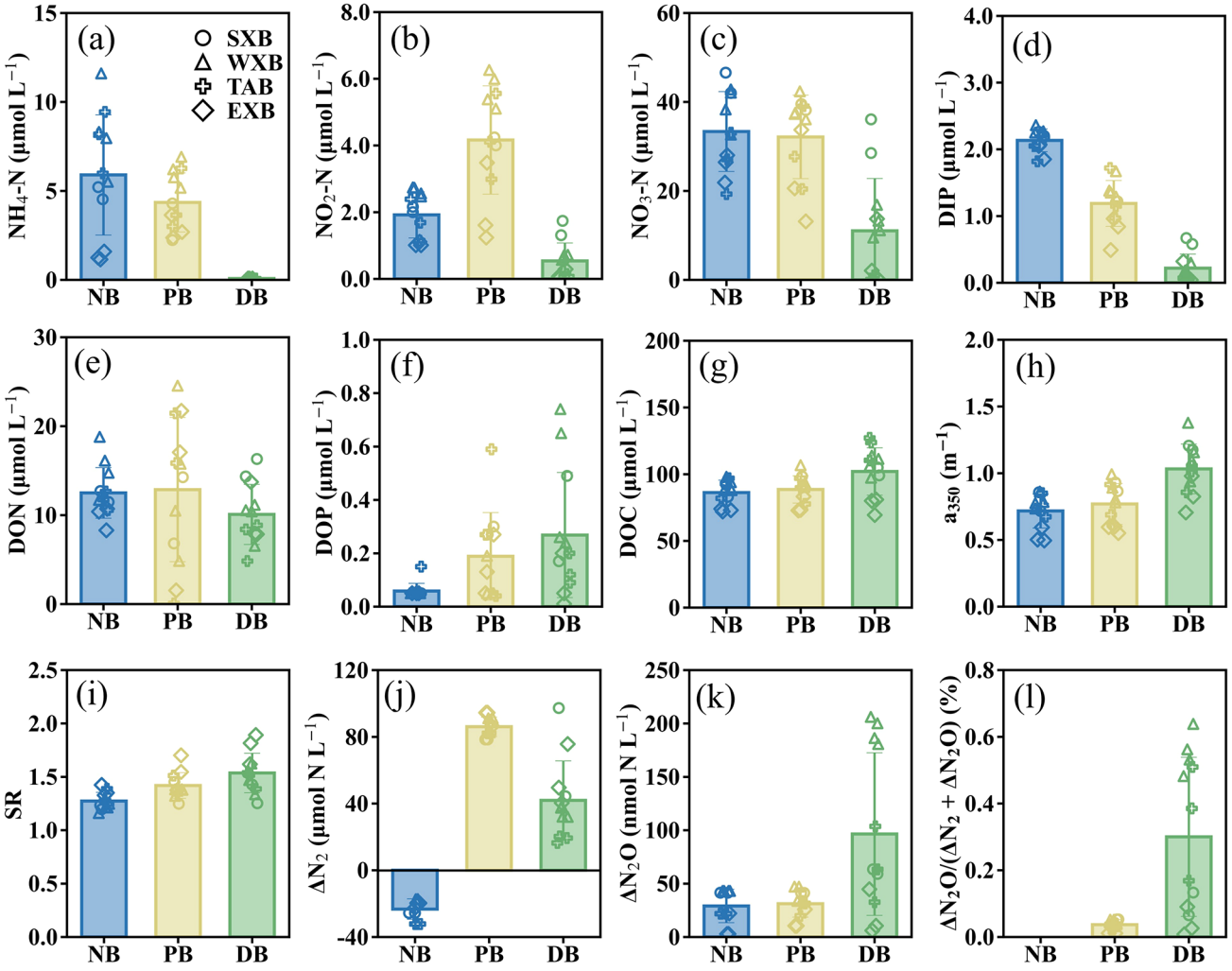


Figure 2. Surface seawater concentrations of dissolved nutrients and gases during the *P. globosa* bloom in Xiamen Bay. ΔN_2 and ΔN_2O denote net deviation from atmospheric equilibrium. NB, PB, and DB refer to the non-bloom, pre-bloom, and during-bloom periods, respectively. Error bars represent standard deviations among sampling sites. SXB, Southern Xiamen Bay; WXB, Western Xiamen Bay; TAB, Tong'an Bay; EXB, Eastern Xiamen Bay.

WXB and TAB, consistent with known bloom-affected zones. No significant spatial gradients were observed for salinity, water temperature, DO, or pH in any period, nor for Eh during NB and PB or Chl *a* during NB.

Sediment geochemistry also exhibited clear temporal evolution (Table S2). Sediment pH was the lowest during NB (6.85 ± 0.16) and increased during both PB (7.85 ± 0.13) and DB (7.82 ± 0.20). In contrast, sediment Eh showed an opposite trend, decreasing from oxidizing conditions during NB (10.28 ± 9.50 mV) to significantly more reduced states during PB (−62.85 ± 7.62 mV) and DB (−61.60 ± 11.69 mV) ($p < 0.001$), with no significant difference between PB and DB ($p > 0.05$). Sedimentary nitrogen pools were altered by the bloom. Total nitrogen (TN) and exchangeable ammonium (NH_4−N) increased progressively from NB to DB. In contrast, total organic carbon (TOC), the molar C/N ratio, and nitrate (NO_3−N) content were the highest during NB, followed by DB and PB.

3.2. Dynamics of Dissolved Nutrients, Organic Matter, and Biogenic Gases

Concentrations of dissolved constituents exhibited pronounced temporal and spatial variability, closely synchronized with bloom progression (Figure 2a-i). Dissolved inorganic nitrogen species (DIN: NH_4−N, NO_3−N) and dissolved inorganic phosphorus (DIP) declined progressively from NB to DB, frequently falling below detection limits during the peak bloom (DB). In contrast, nitrite (NO_2−N) and dissolved organic nitrogen (DON) peaked during PB (NO_2−N: 4.16 ± 1.55 μmol L^{-1}; DON: 12.9 ± 7.77 μmol L^{-1}) before decreasing during DB. Dissolved silicate (DSi) exhibited an opposite trend, with its lowest concentration observed during PB (47.0 ± 7.40 μmol L^{-1}; Figure S4a). Concurrently, DOC, CDOM absorption at 350 nm (a_{350}), and the spectral slope ratio (SR) increased steadily from NB to DB. Spatially, the most pronounced variations across all parameters were concentrated in WXB, SXB, and TAB, corresponding to regions most strongly impacted by the *P. globosa* bloom.

The concentrations and ratios of dissolved biogenic gases changed markedly, reflecting underlying changes in microbial nitrogen transformation pathways (Figure 2j-l). Excess dissolved N_2 (ΔN_2), a proxy for net denitrification, was negative during NB (−23.3 ± 5.86 μmol N L^{-1}), indicating either net N_2 fixation or minimal removal. It became strongly positive during PB (86.0 ± 5.51 μmol N L^{-1}), before declining during DB (41.9 ± 22.6 μmol N L^{-1}). Conversely, excess N_2O (ΔN_2O) increased progressively from NB (29.0 ± 14.9 nmol N L^{-1}) to DB (96.4 ±

https://doi.org/10.1021/acs.est.6c01472
Environ. Sci. Technol. 2026, 60, 20963−20975

Downloaded from pubs.acs.org/esthag/article-pdf/60/30/20963/6601638/acs.est.6c01472.pdf by XIAMEN UNIV user on 16 August 2026

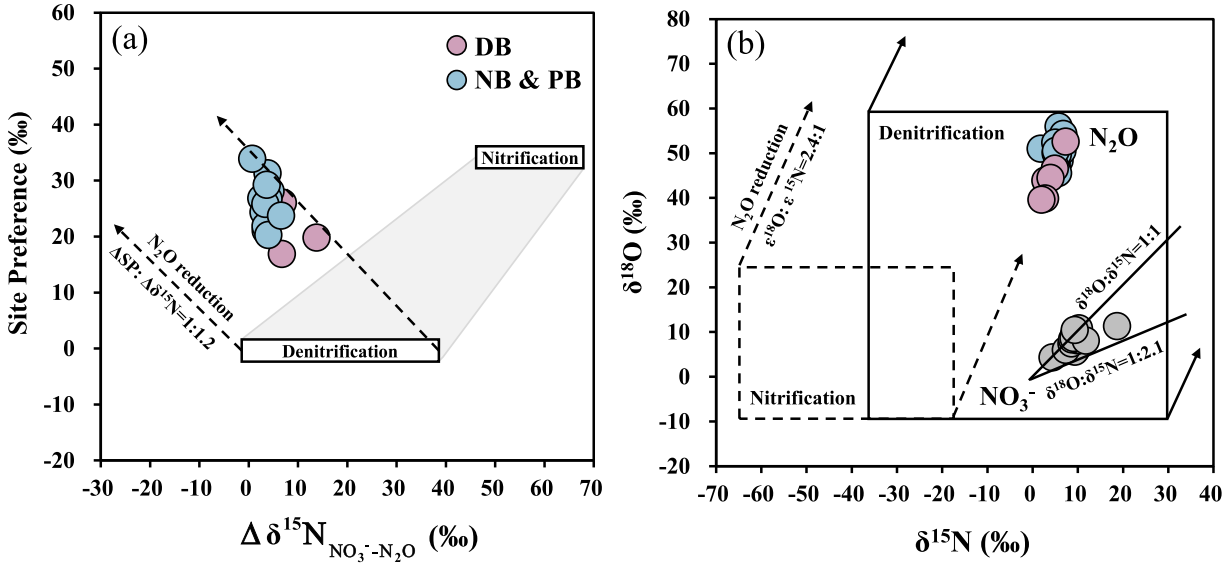


Figure 3. Isotopic characterization of N_2O biogeochemistry in Xiamen Bay. (a) SP-$\Delta\delta^{15}N$ space. Rectangles denote typical isotopic signatures of N_2O derived from nitrification and denitrification. $\Delta\delta^{15}N$ represents the difference in $\delta^{15}N$ between NO_3^- and N_2O. The shaded area indicates mixing of nitrification- and denitrification-derived N_2O, and dashed arrows illustrate the N_2O reduction trajectory. (b) $\delta^{18}O$-$\delta^{15}N$ plot for N_2O and NO_3^-. Solid- and dotted-line areas represent expected isotopic ranges for N_2O from denitrification and nitrification, respectively.[20] Arrows indicate the direction of N_2O reduction and solid lines denote the enrichment trajectory of ^{15}N in NO_3^- during denitrification.[21] NB, PB, and DB refer to the non-bloom, pre-bloom, and during-bloom periods, respectively.

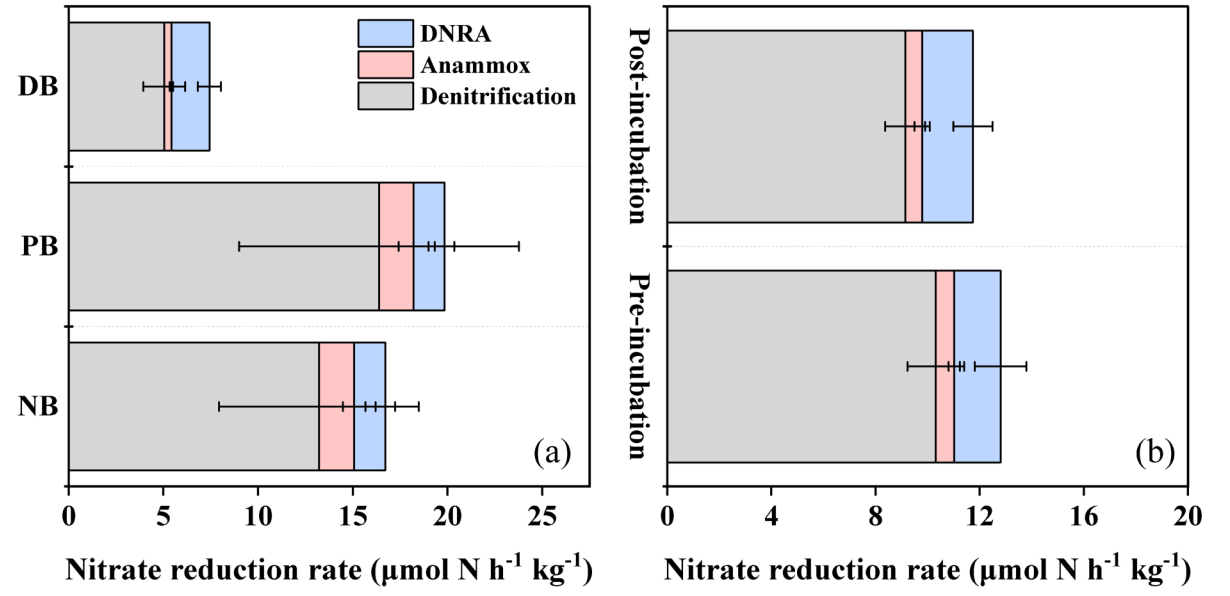


Figure 4. Nitrate reduction rates in sediments across *P. globosa* bloom stages (a) and following bloom-derived algal material amendments (b) in Xiamen Bay. NB, PB, and DB denote the non-bloom, pre-bloom, and during-bloom periods, respectively. Error bars represent standard deviations among sampling sites in (a) and among algal material amendment treatments in (b).

73.0 nmol N L^{-1}), with localized hotspots exceeding 200 nmol N L^{-1} in WXB during DB. Consequently, N_2O yield, defined as $\Delta N_2O/(\Delta N_2 + \Delta N_2O)$, increased significantly from 0.04% ± 0.01% in PB to 0.30% ± 0.23% in DB ($p < 0.01$), representing approximately an order of magnitude increase.

Nutrient stoichiometry also underwent marked reorganization (Figure S5). The molar DIN:DIP ratio increased from 19.0 ± 3.8 (NB) to 45.0 ± 30.0 (DB), except in EXB, where the increase was moderated by lower nitrogen concentrations. In contrast, the DIN:DSi ratio remained relatively stable (~0.85) during NB and PB before declining sharply to 0.19 ± 0.17 in DB, reflecting DIN depletion relative to DSi. Significant empirical relationships emerged among these dynamic pools. The net removal of DIN relative to NB (ΔDIN) was positively correlated with DIP removal (ΔDIP; $R^2 = 0.913$, $p < 0.001$). The change in dissolved organic phosphorus (ΔDOP) exhibited an inverse U-shaped relationship with ΔDOC. Furthermore, total excess gaseous nitrogen ($\Delta N_2 + \Delta N_2O$) showed a significant negative linear correlation with ΔDIN ($R^2 = 0.734$, $p < 0.001$). The N_2O yield, $\Delta N_2O/(\Delta N_2 + \Delta N_2O)$, increased exponentially with ΔDIN ($R^2 = 0.838$, $p < 0.001$), but decreased exponentially with ($\Delta N_2 + \Delta N_2O$) ($R^2 = 0.550$, $p < 0.001$).

https://doi.org/10.1021/acs.est.6c01472
Environ. Sci. Technol. 2026, 60, 20963−20975

Downloaded from pubs.acs.org/esthag/article-pdf/60/30/20963/6601638/acs.est.6c01472.pdf by XIAMEN UNIV user on 16 August 2026

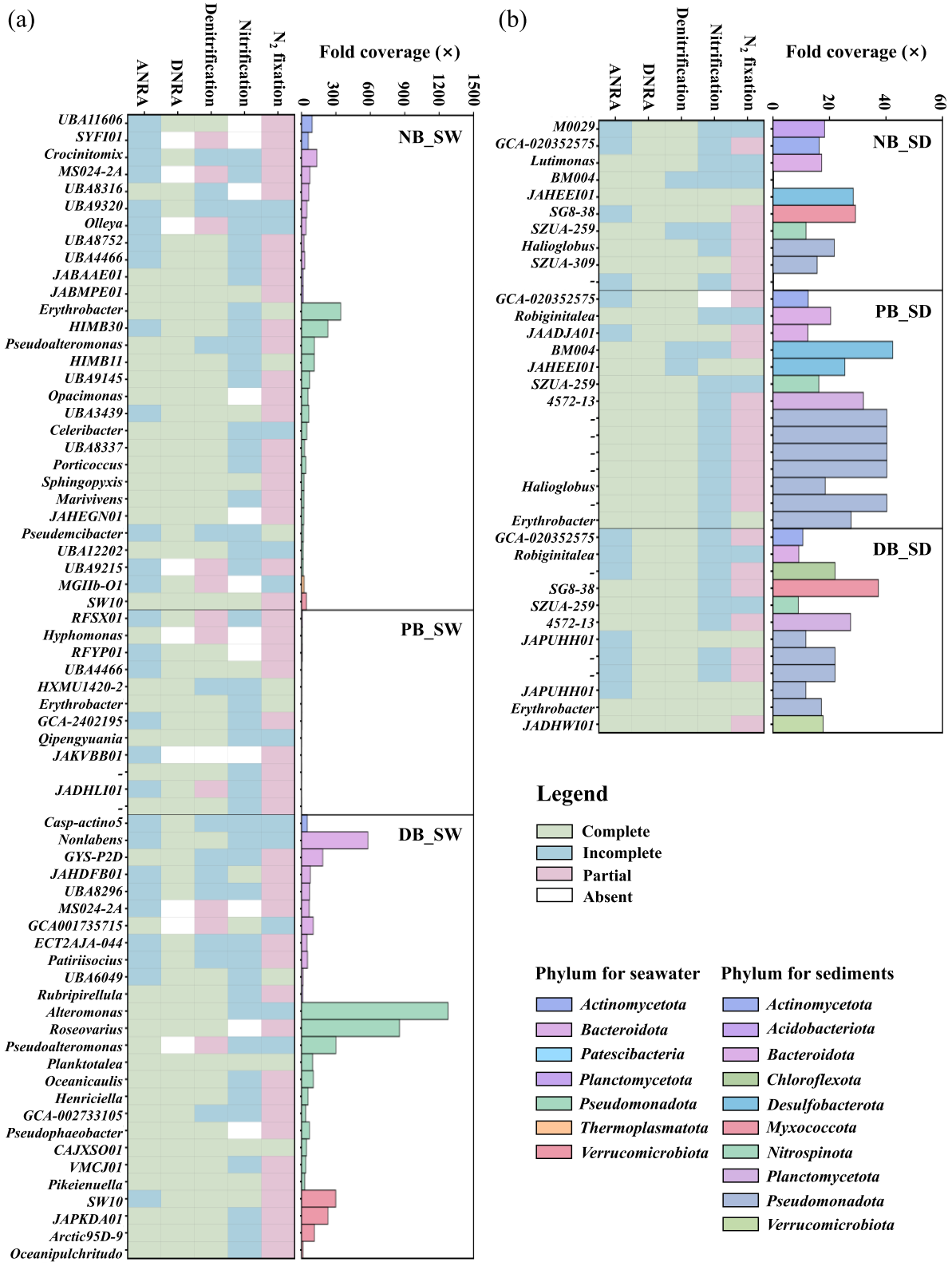


Figure 5. Metabolic pathway completeness, taxonomic annotation, and coverage-based abundance of high-quality MAGs in seawater (a) and sediments (b) during different phases of the *P. globosa* bloom in Xiamen Bay. Heatmaps show nitrogen-cycling pathway completeness and genus-level annotation. Bar plots indicate mean coverage (×) of MAGs. Only MAGs with completeness >70% and contamination <10% are shown. NB, non-bloom; PB, pre-bloom; DB, during-bloom; SW, seawater; SD, sediments.

Downloaded from pubs.acs.org/esthag/article-pdf/60/30/20963/6601638/acs.est.6c01472.pdf by XIAMEN UNIV user on 16 August 2026

https://doi.org/10.1021/acs.est.6c01472
Environ. Sci. Technol. 2026, 60, 20963−20975

3.3. Isotopic Constraints on N_2O Sources and Reduction

The dual-isotope signatures of N_2O are shown in Figure 3. In SP-$\Delta\delta^{15}N$ space (Figure 3a), all samples distributed within or near the denitrification domain, clearly distinct from the high-SP and high-$\Delta\delta^{15}N$ endmember characteristic of nitrification. $\Delta\delta^{15}N$ values remained low across all samples. Compared to NB and PB conditions, bloom samples (DB) exhibited lower SP but higher $\Delta\delta^{15}N$ values. Most data points aligned along the theoretical N_2O reduction trajectory. The minimum estimated contribution of nitrification to total N_2O production was 0% during the bloom and ranged from 0% to 3.51% under NB and PB conditions (Table S3). Accordingly, denitrification accounted for 96.49−100% of total N_2O production. The estimated extent of N_2O reduction was 98.70% ± 0.84% during DB and 99.57% ± 0.33% under NB and PB conditions. In $\delta^{15}N$-$\delta^{18}O$ space (Figure 3b), nitrate exhibited coupled enrichment in $\delta^{15}N$ and $\delta^{18}O$, while N_2O clustered along the transformation pathway from NO_3−N.

3.4. Shifts in Potential Sedimentary Nitrate Reduction Pathways

Incubation experiments revealed shifts in sedimentary nitrate reduction pathways during bloom progression (Figure 4a). During NB, canonical denitrification was the dominant process (13.21 ± 5.27 μmol N h^{-1} kg^{-1}), exceeding rates of anammox (1.86 ± 0.60 μmol N h^{-1} kg^{-1}) and DNRA (1.65 ± 0.40 μmol N h^{-1} kg^{-1}). This pattern persisted into the PB phase. Denitrification further increased to 16.38 ± 7.39 μmol N h^{-1} kg^{-1}, while anammox and DNRA remained relatively stable. The most pronounced changes occurred during DB. Denitrification rates declined sharply by ∼ 70% (to 5.26 ± 1.17 μmol N h^{-1} kg^{-1}), anammox decreased to 0.40 ± 0.10 μmol N h^{-1} kg^{-1}, whereas DNRA increased to 2.01 ± 0.61 μmol N h^{-1} kg^{-1} and increased its relative importance during peak bloom conditions.

Laboratory incubation experiments with bloom-derived algal materials amendments corroborated and extended the field observations (Figure 4b). Over the 7-day incubation, denitrification rates were consistently suppressed in all amended treatments relative to the control, indicating a direct inhibitory effect of *P. globosa*-derived substrates. In contrast, DNRA rates increased slightly from 1.78 ± 0.99 μmol N h^{-1} kg^{-1} to 1.95 ± 0.75 μmol N h^{-1} kg^{-1} following amendment, indicating stimulation of a nitrogen-retention pathway. Anammox rates remained low and showed no statistically significant response to the treatments, underscoring its marginal role under these bloom-influenced conditions.

3.5. Metagenomic Insights into Microbial Communities and Functional Dynamics

The *P. globosa* bloom induced compartmentalized and successional changes in microbial functional potential and taxonomic composition between seawater and sediments (Figures S6, S7). In seawater, the abundances of genes associated with nitrification (*amoABC*, *hao*, *nxrAB*) and denitrification (*narGI*, *napAB*, *nirKS*, *norBC*, *nosZ*) declined during the PB phase relative to NB, with a more consistent reduction observed across denitrification (Figure S6). In contrast, genes encoding assimilatory nitrate reduction (ANRA; e.g., *narB*, *NR*) increased. During DB, denitrification gene abundances rebounded markedly, exceeding NB levels, and DNRA genes (*nirBD*, *nrfAH*) increased but ANRA genes declined. In sediments, genes associated with nitrification, denitrification, and DNRA exhibited an initial increase during PB, followed by a collective decline in DB. Genes diagnostic for anammox (*hzsAB*, *hzo*, *hdh*) were not detected in either compartment.

The bloom elicited more pronounced taxonomic changes in seawater than in sediments (Figure S7). In seawater, the NB community was dominated by denitrifying genera *Pseudoalteromonas* (40.0%) and *Flavobacterium* (11.9%), along with the ammonia-oxidizing archaeon *Nitrosopumilus* (14.9%). The PB phase was characterized by a sharp decline in nitrogen-cycling taxa. *Nitrosopumilus* nearly disappeared (<1.5%) and *Flavobacterium* decreased substantially from 11.9% to 4.5%, whereas *Pseudoalteromonas* became dominant (64.8%). By DB, denitrifying genera increased more than 2-fold. The community became dominated by putative pelagic denitrifiers and sulfur-cycling taxa, including *Erythrobacter* (28.0%), *Roseobacter* (25.4%), *Pseudoalteromonas* (21.7%), and *Ruegeria* (10.1%). Concurrently, sulfur-oxidizing taxa such as *Rhodobacter* and *Paracoccus* increased by ∼12- and 11-fold, respectively, while *Pseudomonas*, associated with assimilatory sulfate reduction, declined markedly (Figure S9). In sediments, nitrogen-cycling communities were dominated by *Nitrosopumilus* (41.7%) and the sulfur-oxidizing, autotrophic denitrifier *Sulfurovum* (29.4%). While *Nitrosopumilus* remained relatively stable, *Sulfurovum* exhibited a clear bloom-associated pattern, reaching a minimum during PB (19.6%) and a maximum during DB (37.7%).

Metagenomic assembly yielded 3154 medium- to high-quality metagenome-assembled genomes (MAGs) across all samples. Subsequent analysis focused on 115 MAGs meeting quality thresholds (>70% completeness and <10% contamination; Figure 5). Assessment of nitrogen-cycling pathway completeness based on KEGG annotation revealed distinct patterns. In seawater, denitrification pathway completeness decreased gradually (NB: 65.5%; PB: 63.6%; DB: 61.5%). DNRA pathways were consistently complete (100%). ANRA completeness was variable (∼50−65%), while nitrification and N_2 fixation pathways were largely incomplete (<27%). In sediments, denitrification pathway completeness increased markedly from PB (79%) to DB (100%). DNRA pathways were also complete (100%) across all periods, while nitrification and N_2 fixation pathways remained low in completeness. Taxonomic annotation using GTDB-Tk indicated bloom-induced changes in phylum-level composition in seawater. *Bacteroidota* and *Pseudomonadota* dominated during NB, nearly disappeared in PB, and recovered in DB alongside the emergence of *Verrucomicrobiota*. In sediments, *Pseudomonadota* increased markedly during PB, becoming the dominant phylum, before declining to near-background levels during DB.

4. DISCUSSION

4.1. Anomalous Warming as the Trigger for a Dry-Season Bloom and Its Biogeochemical Trajectory

The emergence of a major *P. globosa* bloom in late November, during the regional dry season characterized by minimal terrestrial nutrients input (Figure 1c), challenges the conventional eutrophication-centric paradigm for coastal algal blooms. This atypical timing, reminiscent of the first recorded event in 1997, implicates climate-associated forcing, identifying sea surface temperature (SST) as the most plausible driver. A pronounced SST anomaly of ∼3−4 °C above the multidecadal mean (Figure S1b)[18] coincided with the strong 2023−2024 El Niño (Figure 1b) and record-high global SSTs during this period.[22] This warming signal was likely amplified locally by the semi-enclosed topography of Xiamen Bay, restricting heat

Downloaded from pubs.acs.org/esthag/article-pdf/60/30/20963/6601463/acs.est.6c01472.pdf by XIAMEN UNIV user on 16 August 2026

https://doi.org/10.1021/acs.est.6c01472
Environ. Sci. Technol. 2026, 60, 20963−20975

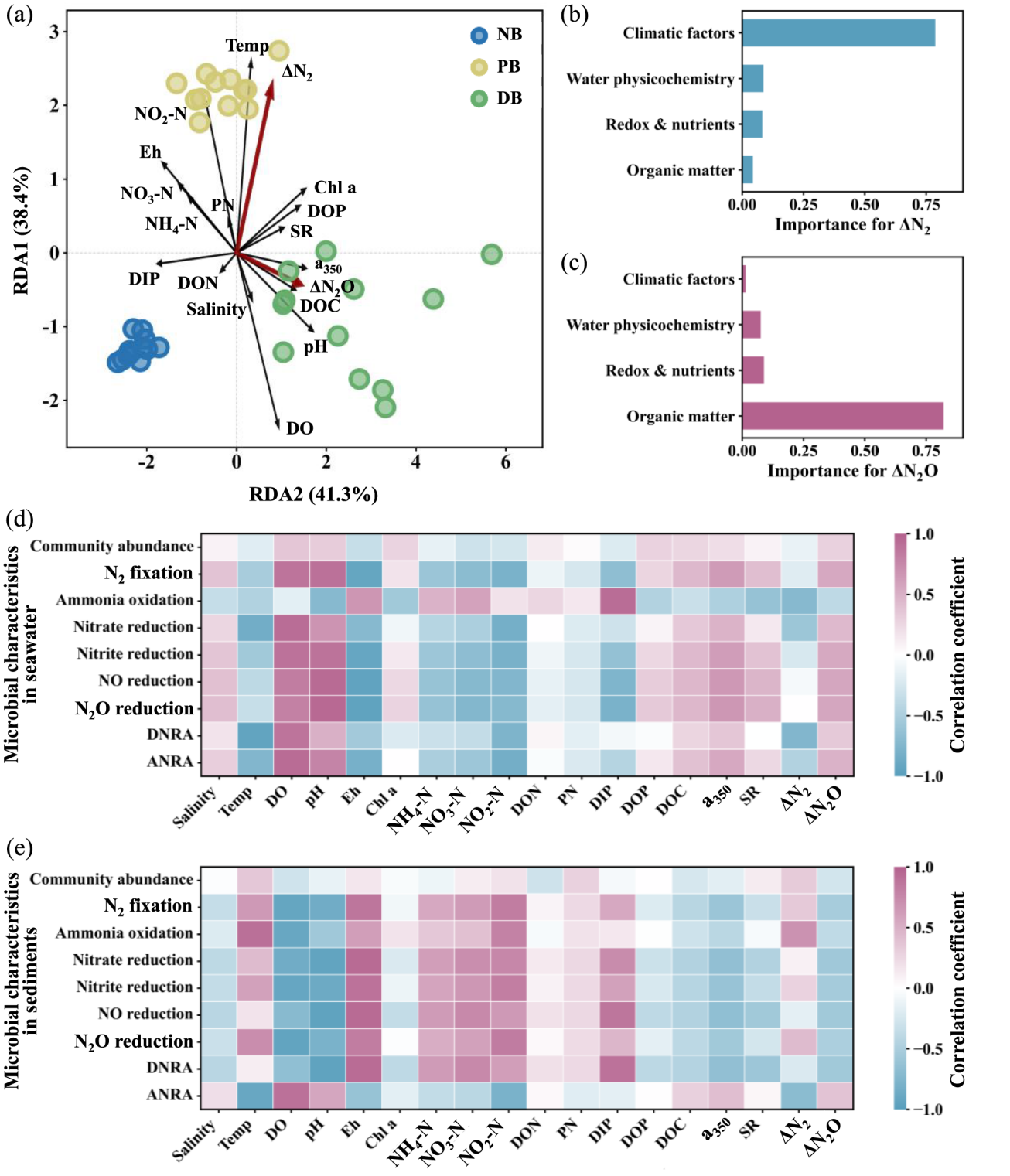


Figure 6. Statistical relationships between environmental variables and microbial indicators across *P. globosa* bloom phases. (a) RDA of environmental factors constraining ΔN_2 and ΔN_2O. (b, c) Random Forest predictor importance for ΔN_2 and ΔN_2O. (d, e) Correlations between environmental factors and metagenomic-derived metrics in seawater and sediments. Predictor variables were grouped into four categories: (i) Climatic factors (water temperature), (ii) Water physicochemistry (salinity, pH, DO), (iii) Redox and nutrients (Eh, NH_4−N, NO_2−N, NO_3−N, DIP), and (iv) Organic matter (Chl *a*, DOC, a_{350}, SR, DON, DOP).

exchange, particularly under reduced freshwater runoff. Such anomalously warm conditions selectively favored *P. globosa*, a thermally tolerant species with optimal growth up to 28 °C and colony formation approaching 31 °C.[23] In contrast, typical local competitors, such as *Akashiwo sanguinea*, thrive near a lower optimum of 25 °C.[24] This physiological advantage likely enabled the rapid proliferation and dominance of *P. globosa* under elevated water temperature conditions. These observations support a hierarchical control wherein large-scale climate forcing sets the thermal boundary conditions, while local hydrographic

https://doi.org/10.1021/acs.est.6c01472
Environ. Sci. Technol. 2026, 60, 20963−20975

Downloaded from pubs.acs.org/esthag/article-pdf/60/30/20963/6601638/acs.est.6c01472.pdf by XIAMEN UNIV user on 16 August 2026

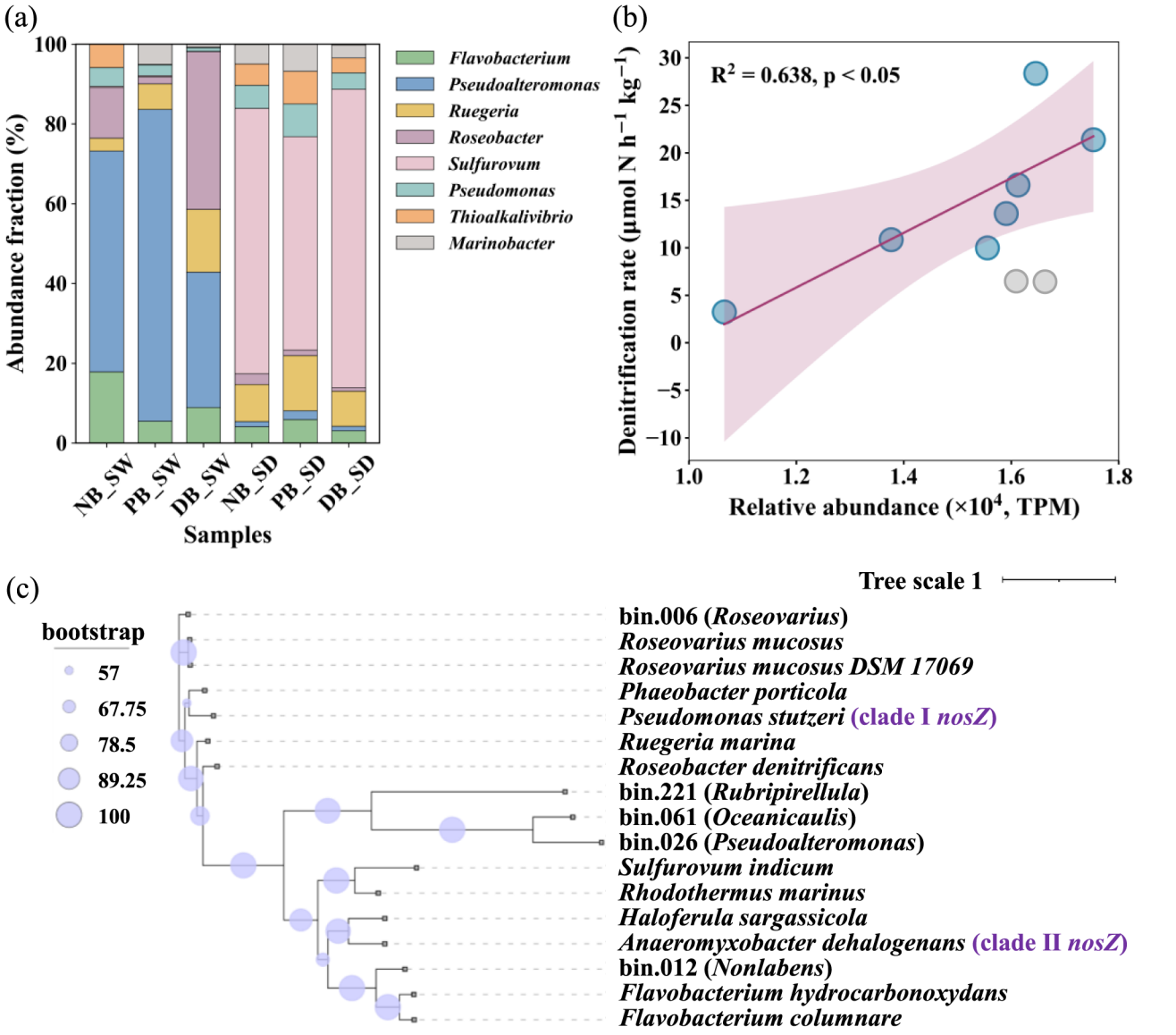


Figure 7. Dynamics of denitrifying communities and process rates during the *P. globosa* bloom in Xiamen Bay. (a) Taxonomic composition of dominant denitrifying taxa (relative abundance >10%) in seawater (SW) and sediments (SD) across bloom phases (NB, PB, DB). (b) Linear regression between sediment denitrification rates and abundances of key functional genes. (c) Phylogenetic reconstruction of *nosZ* gene sequences recovered from seawater and sediments. NB, PB, and DB refer to the non-bloom, pre-bloom, and during-bloom periods, respectively.

constraints amplify this signal, ultimately triggering the species-specific bloom response.

Relative to the multi-year seasonal baseline, water-column conditions during PB and DB deviated substantially from typical seasonal variability (Table S1). During PB, water temperature exceeded the long-term fall mean. Chl *a* concentrations in both periods were several-fold higher than seasonal background levels. Meanwhile, Eh dropped sharply to −139 mV in DB, well below the typical seasonal range of −60 to −68 mV, indicating strongly reducing conditions. These concurrent anomalies in thermal regime, biomass accumulation, and redox state signal a system-level perturbation primarily driven by bloom dynamics, rather than seasonal variability alone. This perturbation followed a clear stage-dependent trajectory, as supported by multivariate analysis. Redundancy analysis (RDA) reveals a transition from a water temperature-regulated regime during PB to an organic matter-dominated system at DB (Figure 6a), reflected by the separation of samples along water temperature and DOC/CDOM vectors. During PB, rising water temperature and Chl *a*, coupled with declining DO (Figure S1) and progressive nutrient depletion (Figure 2), indicate intensified algal growth and system preconditioning. By DB, intense photosynthetic activity drove DO to supersaturation and elevated pH by ∼20% relative to NB conditions. Concurrently, Eh further declined, signaling accumulation of reduced compounds. This redox change is likely due to the production and degradation of algal-derived dimethylsulfoniopropionate (DMSP), leading to the release of dimethyl sulfide (DMS) and other reduced sulfur species, a well-established biochemical hallmark of *P. globosa* blooms.[3,25]

These observations reveal a progression from thermal preconditioning to peak biogeochemical disturbance. This pattern highlights the importance of capturing the full developmental trajectory to understand ecosystem-scale impacts. More broadly, this case shows that climate-driven thermal anomalies can override classical nutrient controls. As a result, bloom dynamics become decoupled from terrestrial inputs,

Downloaded from pubs.acs.org/esthag/article-pdf/60/30/20963/6601463/acs.est.6c01472.pdf by XIAMEN UNIV user on 16 August 2026

https://doi.org/10.1021/acs.est.6c01472
Environ. Sci. Technol. 2026, 60, 20963−20975

redefining the dominant drivers of bloom phenology in subtropical coastal systems.

4.2. Bloom-Induced Impairment of Pelagic Denitrification and Enhancement of N_2O Emission in Seawater

Our integrated data set challenges the prevailing paradigm that algal blooms stimulate denitrification. The *P. globosa* bloom instead severely impaired this key nitrogen-removal pathway and redirected gaseous nitrogen emissions toward N_2O. The massive algal proliferation caused a pronounced drawdown of DIN and DIP. Concentrations of NH_4−N, NO_3−N, and DIP declined progressively from NB to DB and often fell below detection limits during DB (Figure 2a-d). Relative to NB baselines, total removal averaged ∼30 μmol L^{-1} for DIN and ∼2.87 μmol L^{-1} for DIP, respectively. This substrate depletion suppressed the system's denitrification capacity, as evidenced by the significant negative correlation between ($\Delta N_2 + \Delta N_2O$) and cumulative DIN removal (Figure S5d). Despite this suppression, the composition of gaseous nitrogen loss became increasingly dominated by N_2O. Random Forest analysis reveals that ΔN_2 is primarily regulated by climatic factor (notably water temperature), whereas ΔN_2O variability is overwhelmingly controlled by organic matter (Figure 6b,c). This divergence indicates a decoupling between total nitrogen removal and its gaseous end-product structure under bloom conditions. Accordingly, N_2O yield increased by approximately an order of magnitude, from 0.04% in PB to 0.30% in DB (Figure 2l). Dual-isotope tracing further constrains the origin of this N_2O. Consistently low SP values and $\Delta\delta^{15}N$ signatures, along with a negligible minimum contribution from nitrification (0−3.51%), demonstrate that N_2O was derived predominantly from denitrification (Figure 3). These results indicate that the increase in N_2O yield is linked to alterations in the product partitioning of denitrification (N_2 vs N_2O), rather than a change in the dominant nitrogen transformation pathway.

This apparent paradox, active denitrification-derived N_2O production under highly oxygenated bulk conditions, can be explained by microscale redox heterogeneity. This heterogeneity allows denitrification to persist independently of bulk oxygen conditions. Despite elevated ambient DO from intense photosynthesis, oxygen-depleted microenvironments likely formed within particulate microhabitats,[26−28] such as *P. globosa* colonies, organic aggregates and suspended particles. Within these microhabitats, high microbial respiration and restricted diffusion sustain steep oxygen gradients, creating localized anoxic niches for denitrification. These microscale environments not only permit denitrification but also bias its end-product composition toward N_2O. At oxic-anoxic interfaces, elevated pH and supersaturated DO inhibit N_2O reductase activity, promoting N_2O accumulation.[29,30] This inhibition likely represents a primary control on N_2O accumulation in bloom waters.

Superimposed on this inhibition of N_2O reduction, a key contributing factor is the release of organic matter (DOC/CDOM) during the bloom (Figure 6), particularly reduced sulfur compounds from *P. globosa*. These compounds, such as DMSP and its degradation products, likely contributed to the restructuring of the pelagic denitrifier community. The typical marine heterotrophic denitrifiers like *Pseudoalteromonas* and *Flavobacterium* were replaced by sulfur-metabolizing taxa such as *Roseobacter* (Figure 7a), which couple sulfur oxidation to nitrate reduction. Consistently, sulfur oxidation-related genes (e.g., *soxAYZB*, *fccAB*, *doxDA*) were enriched during the bloom, indicating enhanced oxidation of reduced sulfur compounds that can serve as electron donors for sulfur-coupled denitrification. The restructured community is further characterized by increased representation of organisms harboring clade I *nosZ* (Figure 7c). This variant is more sensitive to oxygen and pH and exhibits reduced N_2O reduction under these conditions compared to clade II.[31] In addition, accumulation of reduced sulfur intermediates (e.g., H_2S derived from DMS transformation) may also inhibit *nosZ* expression and enzymatic activity.[32,33] Thus, these sulfur-driven microbial processes reinforce N_2O accumulation in the pelagic system.

Together, the combined effects of substrate limitation, environmental inhibition of N_2O reduction, and sulfur-mediated microbial restructuring reduce N_2 production while promoting N_2O accumulation. The increase in N_2O yield is primarily governed by inhibition of the N_2O reduction step, whereas substrate limitation constrains total nitrogen removal and sulfur-mediated microbial restructuring acts as a reinforcing mechanism that further amplifies N_2O accumulation. Rather than reflecting a shift in dominant nitrogen transformation pathways, this pattern indicates a fundamental change in process efficiency, with climate-driven blooms regulating the completeness of denitrification rather than its occurrence.

4.3. Decoupled Sedimentary Response: Thermal Enhancement Preceding Sulfur-Mediated Metabolic Constraint

In contrast to the pelagic zone, sedimentary denitrification exhibited a temporally decoupled response, with N_2 emissions peaking during PB, prior to DB. This early maximum is consistent with statistical analyses, which identify water temperature as the dominant predictor of ΔN_2 (Figure 6). This pattern indicates a kinetically controlled, thermally regulated regime of benthic nitrogen removal. This thermal enhancement was accompanied by a pronounced microbial response. The coverage-based abundance of key denitrifying MAGs approximately doubled during PB (Figure 5b). This increase coincided with the highest potential denitrification rates (Figure 4a) under favorable sediment geochemical conditions, including elevated pH, reduced Eh, and low C/N ratio (Table S2).[34] However, this water temperature-driven regime was abruptly disrupted during DB, when denitrification rates dropped to ∼40% of the nonbloom baseline (Figure 4a), indicating a clear mechanistic transition. We attribute this reversal to bloom-induced organic matter deposition, associated with a sulfur-mediated metabolic reorganization in sediments. Elevated concentrations of DOC and CDOM signaled enhanced sedimentation of algal-derived material. This interpretation is supported by microcosm incubations showing that addition of algal residue significantly reduced denitrification rates in 7-day batch assays (∼11.3%, $p < 0.05$, Figure 4b).

Metagenomic evidence indicates that this organic matter pulse was coupled with a restructuring of sulfur cycling pathways. During DB, genes associated with assimilatory sulfate reduction (e.g., *cys*, *sir*) increased, while dissimilatory pathways (e.g., *dsrAB*, *aprAB*, *sat*) declined. This pattern suggests intensified sulfur incorporation into biomass and likely reflects the subsequent production of reduced sulfur intermediates during organic matter degradation. These reduced sulfur compounds (e.g., sulfide, thiosulfate) provide electron donors for chemolithoautotrophic sulfur-oxidizers, promoting sulfur-driven metabolism. Consistent with this, the sulfur-oxidizing genus *Sulfurovum* dominated the sedimentary denitrifier

Downloaded from pubs.acs.org/esthag/article-pdf/60/30/20963/6601638/acs.est.6c01472.pdf by XIAMEN UNIV user on 16 August 2026

https://doi.org/10.1021/acs.est.6c01472
Environ. Sci. Technol. 2026, 60, 20963−20975

community and further increased in relative abundance from ~53% to 75% during DB. This increase was likely fueled by labile organic sulfur compounds derived from DMSP-rich algal detritus.[35,36] As a result, chemolithoautotrophic denitrification was favored but exhibited lower rates. This likely reflects greater energetic constraints relative to heterotrophic pathways.[37,38] Consequently, the system transitioned from a water temperature-enhanced, heterotrophy-dominated regime (PB) to a sulfur-driven regime (DB), resulting in a marked reduction in overall denitrification capacity. Despite this suppression, sedimentary N_2O accumulation remained limited. This constraint is likely due to the dominance of organisms harboring *nosZ* clade II (Figure 7c), a genotype commonly associated with more efficient N_2O reduction under these conditions.[39] This pattern contrasts sharply with the overlying seawater, where *nosZ* clade I dominance promotes N_2O accumulation (Section 4.2), highlighting a compartmentalized divergence in nitrogen transformation pathways.

In summary, these results reveal a compartmentalized and decoupled response of coastal nitrogen cycling to bloom perturbation. While seawater exhibits organic matter- and sulfur-driven enhancement of N_2O production, sediments display sulfur-mediated metabolic constraint of denitrification. This divergence reflects a transition from kinetic to metabolic control. This transition ultimately weakens the ecosystem's nitrogen removal capacity, highlighting how climate-driven blooms can disrupt biogeochemical functions through phase-specific microbial mechanisms.

4.4. Implications

A central finding of this study is that climate-driven harmful algal blooms induce a spatially decoupled yet functionally integrated response between seawater and sediments, collectively impairing the coastal nitrogen filter. Although both compartments are subjected to the same bloom-derived organic matter and sulfur inputs, their responses diverge fundamentally. In seawater, elevated organic matter availability and oxygenated conditions inhibit N_2O reduction, leading to substantial N_2O accumulation. In contrast, sediments favor sulfur-driven chemolithoautotrophic denitrification, which constrains overall N_2 production. This cross-compartment divergence decouples nitrogen removal from its gaseous end products, reducing N_2 production while enhancing N_2O yield at the system level.

The increase in N_2O yield is primarily governed by suppression of the N_2O reduction step, rather than a shift in dominant nitrogen transformation pathways. Isotopic evidence indicates that denitrification remains the dominant source of N_2O, indicating that pathway structure is largely preserved. Instead, bloom-induced environmental conditions, particularly elevated oxygen and pH in seawater, truncate the denitrification pathway by inhibiting N_2O reductase activity. Substrate limitation further constrains total nitrogen removal, while sulfur-mediated microbial restructuring acts as a reinforcing mechanism that amplifies N_2O accumulation. Together, these processes reduce the completeness of denitrification rather than its occurrence.

These findings challenge the prevailing carbon-centric paradigm of bloom-driven nitrogen cycling. Rather than uniformly enhancing denitrification through increased labile carbon supply,[10−12,40−42] the impact of algal blooms depends on bloom functional identity and associated biogeochemical forcing. In this case, sulfur-mediated microbial processes emerge as a key regulator of denitrification efficiency and N_2O yield. This study establishes a conceptual framework in which climate-driven blooms alter not only the magnitude but also the efficiency of nitrogen removal. Under warming scenarios that favor HAB species such as *P. globosa*, coastal ecosystems may transition from effective nitrogen filters to coupled hotspots of nitrogen retention and N_2O emission. Incorporating microbial functional traits and sulfur cycling into biogeochemical models will therefore be essential for predicting coastal feedbacks to climate change.

■ ASSOCIATED CONTENT

Supporting Information

The Supporting Information is available free of charge at https://pubs.acs.org/doi/10.1021/acs.est.6c01472.

Detailed experimental methods including Chl *a* measurement, slurry incubation, bloom-residue amendment experiment, DNA extraction and metagenomic analysis, semiquantitative analysis of N_2O source partitioning, and statistical analyses; physicochemical parameters, Chl *a*, and stoichiometric diagnostics during different bloom phases; heat maps and bar plots of nitrogen- and sulfur-cycling microorganisms in seawater and sediments; sediment physicochemical properties; N_2O source contributions and reduction ratio; and seasonal baseline of physicochemical parameters and nitrogen removal rates in Xiamen Bay (2019−2023) (PDF)

■ AUTHOR INFORMATION

Corresponding Authors

Fan Qu − *Fujian Provincial Key Laboratory for Coastal Ecology and Environmental Studies, College of the Environment and Ecology, Xiamen University, Xiamen 361102, P. R. China; National and Local Joint Engineering Research Center of Ecological Treatment Technology for Urban Water Pollution, College of Life and Environmental Science, Wenzhou University, Wenzhou 325035, P. R. China*; Email: 20250103@wzu.edu.cn

Nengwang Chen − *State Key Laboratory of Marine Environmental Science, Xiamen University, Xiamen 361102, P. R. China; Fujian Provincial Key Laboratory for Coastal Ecology and Environmental Studies, College of the Environment and Ecology, Xiamen University, Xiamen 361102, P. R. China*; orcid.org/0000-0002-5200-1035; Email: nwchen@xmu.edu.cn

Authors

Mingzhen Zhang − *State Key Laboratory of Marine Environmental Science, Xiamen University, Xiamen 361102, P. R. China; Fujian Provincial Key Laboratory for Coastal Ecology and Environmental Studies, College of the Environment and Ecology, Xiamen University, Xiamen 361102, P. R. China*

Yiqi Yu − *State Key Laboratory of Marine Environmental Science, Xiamen University, Xiamen 361102, P. R. China; Fujian Provincial Key Laboratory for Coastal Ecology and Environmental Studies, College of the Environment and Ecology, Xiamen University, Xiamen 361102, P. R. China*

Xiyu Zhang − *State Key Laboratory of Marine Environmental Science, Xiamen University, Xiamen 361102, P. R. China; Fujian Provincial Key Laboratory for Coastal Ecology and Environmental Studies, College of the Environment and Ecology, Xiamen University, Xiamen 361102, P. R. China*

Downloaded from pubs.acs.org/esthag/article-pdf/60/30/20963/6601638/acs.est.6c01472.pdf by XIAMEN UNIV user on 16 August 2026

Complete contact information is available at:
https://pubs.acs.org/10.1021/acs.est.6c01472

Notes

The authors declare no competing financial interest.

■ ACKNOWLEDGMENTS

This study was supported by the National Natural Science Foundation of China Youth Basic Research Project (No. 424B2052), the National Natural Science Foundation of China (No. 42530405), and the PhD Fellowship of the State Key Laboratory of Marine Environmental Science at Xiamen University. We thank Junou Du and Shaowei Zheng for their assistance in field and laboratory work.

■ REFERENCES

(1) Dai, Y. H.; Yang, S. B.; Zhao, D.; Hu, C. M.; Xu, W.; Anderson, D. M.; Li, Y.; Song, X. P.; Boyce, D. G.; Gibson, L.; Zheng, C. M.; Feng, L. Coastal phytoplankton blooms expand and intensify in the 21st century. *Nature* **2023**, *615* (7951), 280−284.
(2) Zhu, Z.; Meng, R.; Smith, W. O., Jr.; Doan-Nhu, H.; Nguyen-Ngoc, L.; Jiang, X. Bacterial composition associated with giant colonies of the harmful algal species *Phaeocystis globosa*. *Front. Microbiol.* **2021**, *12*, No. e737484.
(3) Royer, C.; Borges, A. V.; Lapeyra Martin, J.; Gypens, N. Drivers of the variability of dimethylsulfoniopropionate (DMSP) and dimethylsulfoxide (DMSO) in the Southern North Sea. *Cont. Shelf Res.* **2021**, *216*, 104360.
(4) Klintzsch, T.; Langer, G.; Nehrke, G.; Wieland, A.; Lenhart, K.; Keppler, F. Methane production by three widespread marine phytoplankton species: Release rates, precursor compounds, and potential relevance for the environment. *Biogeosciences* **2019**, *16* (20), 4129−4144.
(5) Hoogstraten, A.; Peters, M.; Timmermans, K. R.; de Baar, H. J. W. Combined effects of inorganic carbon and light on *Phaeocystis globosa Scherffel* (*Prymnesiophyceae*). *Biogeosciences* **2012**, *9* (5), 1885−1896.
(6) Mars Brisbin, M.; Mitarai, S.; Saito, M. A.; Alexander, H. Microbiomes of bloom-forming *Phaeocystis* algae are stable and consistently recruited, with both symbiotic and opportunistic modes. *ISME J.* **2022**, *16* (9), 2255−2264.
(7) Chen, N. S.; Xu, Q.; Zhu, J. N.; Song, H. Y.; He, L. Y.; Liu, S. Y.; Song, X. X.; Yuan, Y. Q.; Chen, Y.; Cao, X. H.; Yu, Z. M. Chromosome-scale genome assembly reveals insights into the evolution and ecology of the harmful algal bloom species *Phaeocystis globosa Scherffel*. *iScience* **2024**, *27* (8), 110575.
(8) Seitzinger, S.; Harrison, J. A.; Böhlke, J. K.; Bouwman, A. F.; Lowrance, R.; Peterson, B.; Tobias, C.; Van Drecht, G. Denitrification across landscapes and waterscapes: A synthesis. *Ecol. Appl.* **2006**, *16* (6), 2064−2090.
(9) Wrage, N.; Velthof, G. L.; van Beusichem, M. L.; Oenema, O. Role of nitrifier denitrification in the production of nitrous oxide. *Soil Biol. Biochem.* **2001**, *33* (12), 1723−1732.
(10) Huang, Y. Y.; Chen, X. C.; Ostrovsky, I. Cyanobacterial blooms enhance nitrogen removal in lakes through carbon/nitrogen coupling metabolism. *ACS EST Water* **2023**, *3* (10), 3244−3252.
(11) Lu, C. C.; Xie, Z.; Guo, J. B.; Song, Y. Y.; Xing, Y. J.; Han, Y.; Li, H. B.; Hou, Y. N. Chlorophyll as natural redox mediators for the denitrification process. *Int. Biodeterior. Biodegrad.* **2020**, *148*, 104895.
(12) Tan, E. H.; Zou, W. B.; Jiang, X. L.; Wan, X. H.; Hsu, T. C.; Zheng, Z. Z.; Chen, L.; Xu, M.; Dai, M. H.; Kao, S. J. Organic matter decomposition sustains sedimentary nitrogen loss in the Pearl River Estuary, China. *Sci. Total Environ.* **2019**, *648*, 508−517.
(13) Song, L. Y. A multiomics approach to study the microbiome response to phytoplankton blooms. *Appl. Microbiol. Biotechnol.* **2017**, *101* (12), 4863−4870.
(14) Buchan, A.; LeCleir, G. R.; Gulvik, C. A.; González, J. M. Master recyclers: Features and functions of bacteria associated with phytoplankton blooms. *Nat. Rev. Microbiol.* **2014**, *12* (10), 686−698.
(15) Chen, B. H.; Wang, K.; Dong, X.; Lin, H. Long-term changes in red tide outbreaks in Xiamen Bay in China from 1986 to 2017. *Estuar. Coast. Shelf Sci.* **2021**, *249*, No. 107095.
(16) Yu, D.; Yan, W. J.; Chen, N. W.; Peng, B. R.; Hong, H. S.; Zhuo, G. H. Modeling increased riverine nitrogen export: Source tracking and integrated watershed-coast management. *Mar. Pollut. Bull.* **2015**, *101* (2), 642−652.
(17) Cheng, P.; Wang, A. J.; Wu, J. Z.; Lin, Y. H.; Chen, J. X.; Chen, N. W. An assessment of residence and influence times in Xiamen Bay, China. *Estuarine, Coastal Shelf Sci.* **2021**, *262*, 107595.
(18) Zhang, M. Z.; Yu, D.; Yu, Y. Q.; Yan, R. F.; Li, Y. S.; Gong, W. J.; Xiao, K.; Li, S. B.; Chen, N. W. Drought reduces nitrogen supply and N_2O emission in coastal bays. *Water Res.* **2024**, *266*, 122362.
(19) Sigman, D. M.; Casciotti, K. L.; Andreani, M.; Barford, C.; Galanter, M.; Böhlke, J. K. A bacterial method for the nitrogen isotopic analysis of nitrate in seawater and freshwater. *Anal. Chem.* **2001**, *73* (17), 4145−4153.
(20) Koba, K.; Osaka, K.; Tobari, Y.; Toyoda, S.; Ohte, N.; Katsuyama, M.; Suzuki, N.; Itoh, M.; Yamagishi, H.; Kawasaki, M.; Kim, S. J.; Yoshida, N.; Nakajima, T. Biogeochemistry of nitrous oxide in groundwater in a forested ecosystem elucidated by nitrous oxide isotopomer measurements. *Geochim. Cosmochim. Acta* **2009**, *73* (11), 3115−3133.
(21) Kendall, C. Tracing nitrogen sources and cycling in catchments. In *Isotope tracers in catchment hydrology*; Kendall, C.; McDonnell, J. J. eds., Amsterdam: Elsevier; 1998, pp. 519−576.
(22) Terhaar, J.; Burger, F. A.; Vogt, L.; Frölicher, T. L.; Stocker, T. F. Record sea surface temperature jump in 2023−2024 unlikely but not unexpected. *Nature* **2025**, *639* (8056), 942−946.
(23) Sun, Y. F.; Wang, Y. Y.; Lei, J.; Qian, C. C.; Zhu, X. X.; Akbar, S.; Huang, Y.; Yang, Z. Temperature-dependent elimination efficiency on *Phaeocystis globosa* by different initial population sizes of *rotifer Brachionus plicatilis*. *Chemosphere* **2018**, *203*, 474−481.
(24) Matsubara, T.; Nagasoe, S.; Yamasaki, Y.; Shikata, T.; Shimasaki, Y.; Oshima, Y.; Honjo, T. Effects of temperature, salinity, and irradiance on the growth of the dinoflagellate *Akashiwo sanguinea*. *J. Exp. Mar. Biol. Ecol.* **2007**, *342* (2), 226−230.
(25) Chen, J. P.; Lin, Y.; Dai, Y. T.; Li, W. J.; Huang, L. L.; Shen, H.; Yang, X.; Ding, S.; Liang, B. B.; Li, L.; Deng, X. W.; Gao, Q. Sulfate-dependent mechanisms of dimethyl sulfide release in freshwater ecosystems: Evidence from field and experimental studies. *Environ. Sci. Technol.* **2025**, *59* (20), 10001−10009.
(26) Wan, X. H.; Sheng, H.-X.; Liu, L.; Shen, H.; Tang, W. Y.; Zou, W. B.; Xu, M. N.; Zheng, Z. Z.; Tan, E. H.; Chen, M. M.; et al. Particle-associated denitrification is the primary source of N_2O in oxic coastal waters. *Nat. Commun.* **2023**, *14* (1), 8280.
(27) Bianchi, D.; Weber, T. S.; Kiko, R.; Deutsch, C. Global niche of marine anaerobic metabolisms expanded by particle microenvironments. *Nat. Geosci.* **2018**, *11* (4), 263−268.
(28) Broman, E.; Zilius, M.; Samuiloviene, A.; Vybernaite-Lubiene, I.; Politi, T.; Klawonn, I.; Voss, M.; Nascimento, F. J. A.; Bonaglia, S. Active DNRA and denitrification in oxic hypereutrophic waters. *Water Res.* **2021**, *194*, 116954.
(29) Kampschreur, M. J.; Temmink, H.; Kleerebezem, R.; Jetten, M. S. M.; van Loosdrecht, M. C. M. Nitrous oxide emission during wastewater treatment. *Water Res.* **2009**, *43* (17), 4093−4103.
(30) Pan, Y. T.; Ye, L.; Ni, B. J.; Yuan, Z. G. Effect of pH on N_2O reduction and accumulation during denitrification by methanol utilizing denitrifiers. *Water Res.* **2012**, *46* (15), 4832−4840.
(31) Suenaga, T.; Hori, T.; Riya, S.; Hosomi, M.; Smets, B. F.; Terada, A. Enrichment, isolation, and characterization of high-affinity N_2O-reducing bacteria in a gas-permeable membrane reactor. *Environ. Sci. Technol.* **2019**, *53* (20), 12101−12112.
(32) Kiene, R. P.; Linn, L. J. The fate of dissolved dimethylsulfoniopropionate (DMSP). in seawater: Tracer studies using ^{35}S-DMSP. *Geochim. Cosmochim. Acta* **2000**, *64* (16), 2797−2810.

Downloaded from pubs.acs.org/esthag/article-pdf/60/30/20963/6601638/acs.est.6c01472.pdf by XIAMEN UNIV user on 16 August 2026

(33) Pan, Y.; Ye, L.; Yuan, Z. Effect of H_2S on N_2O reduction and accumulation during denitrification by methanol utilizing denitrifiers. *Environ. Sci. Technol.* **2013**, *47* (15), 8408−8415.
(34) Zhu, X.; Yang, F.; Pang, Q. Q.; Peng, F. Q.; Xu, B.; Wang, L. M.; Xie, L.; Zhang, W. H.; Tian, L. F.; Hou, J.; Zhou, C.; Hu, Z. F. Fluvial dissolved organic matter quality modulates microbial nitrate transformation: Enhanced denitrification under low carbon-to-nitrate ratio. *Environ. Sci. Technol.* **2025**, *59* (43), 23456−23465.
(35) Campbell, B. J.; Engel, A. S.; Porter, M. L.; Takai, K. The versatile ε-proteobacteria: Key players in sulphidic habitats. *Nat. Rev. Microbiol.* **2006**, *4* (6), 458−468.
(36) Jiang, H.; Jiang, M.; Zhang, Q. F. Coupled sulfur and nitrogen cycling at a catchment scale: Insights from isotopic and molecular techniques. *Water Res.* **2024**, *267*, 122438.
(37) Hu, Y. S.; Wu, G. X.; Li, R. H.; Xiao, L. W.; Zhan, X. M. Iron sulphides mediated autotrophic denitrification: An emerging bioprocess for nitrate pollution mitigation and sustainable wastewater treatment. *Water Res.* **2020**, *179*, 115914.
(38) Shao, M. F.; Zhang, T.; Fang, H. H. P. Sulfur-driven autotrophic denitrification: Diversity, biochemistry, and engineering applications. *Appl. Microbiol. Biotechnol.* **2010**, *88* (5), 1027−1042.
(39) Yang, W.; Zhao, Q.; Lu, H.; Ding, Z.; Meng, L.; Chen, G.-H. Sulfide-driven autotrophic denitrification significantly reduces N_2O emissions. *Water Res.* **2016**, *90*, 176−184.
(40) Shen, Y. S.; Huang, Y. Y.; Hu, J. L.; Li, P.; Zhang, C.; Li, L. X.; Xu, P. Z. J.; Zhang, J.; Chen, X. The nitrogen reduction in eutrophic water column driven by *Microcystis* blooms. *J. Hazard. Mater.* **2020**, *385*, No. e121578.
(41) Ji, Y. Y.; Shi, W. Q.; Brookes, J.; Qin, B. Q. A heterogeneity of water and sediment nitrogen removal patterns in shallow lakes: Implications for lake management. *J. Environ. Manage.* **2025**, *389*, 126167.
(42) Jiang, X. Y.; Liu, C. Q.; Cai, J.; Hu, Y.; Shao, K. Q.; Tang, X. M.; Gong, Y.; Yao, X. L.; Xu, Q. J.; Gao, G. Relationships between environmental factors and N-cycling microbes reveal the indirect effect of further eutrophication on denitrification and DNRA in shallow lakes. *Water Res.* **2023**, *245*, 120572.

Downloaded from pubs.acs.org/esthag/article-pdf/60/30/20963/6601463/acs.est.6c01472.pdf by XIAMEN UNIV user on 16 August 2026

https://doi.org/10.1021/acs.est.6c01472
Environ. Sci. Technol. 2026, 60, 20963−20975